Direct observation of chemical reactions on single gold nanocrystals using surface plasmon spectroscopy

CAROLINA NOVO, ALISON M. FUNSTON AND PAUL MULVANEY*

School of Chemistry & Bio21 Institute, University of Melbourne, Parkville, Vic. 3010, Australia
***e-mail: mulvaney@unimelb.edu.au**

Published online: 14 September 2008; doi:10.1038/nnano.2008.246

Heterogeneous catalysts have been pivotal to the development of the modern chemical industry and are essential for catalysing many industrial reactions. However, reaction rates are different for every individual catalyst particle and depend upon each particle's morphology and size[1], crystal structure[2] and composition[3–7]. Measuring the rates of reaction on single nanocrystals will enable the role of catalyst structure to be quantified. Here, using surface plasmon spectroscopy, we have directly observed the kinetics of atomic deposition onto a single gold nanocrystal and also monitored electron injection and extraction during a redox reaction involving the oxidation of ascorbic acid on a gold nanocrystal surface. These results constitute the first direct measurement of the rates of redox catalysis on single nanocrystals.

The *in situ* measurement of reaction rates in heterogeneous catalysis remains a fundamental challenge[8]. There are two profound difficulties. The first is monitoring reaction rates on catalyst surfaces in real time so that reaction mechanisms can be elucidated. Increasingly sophisticated methods are being applied. For example, Gates and colleagues have used time resolved IR spectroscopy to study the oxidation of carbon monoxide on gold catalyst surfaces[7]. However, as such measurements are ensemble averages, they do not allow one to correlate catalytic activity with particular types of particle present. Thus, a second major barrier to progress is the need to understand the relationship between the nanocrystal structure and its catalytic activity. To surmount this difficulty, catalytic studies on single nanocrystals of well-defined shape and structure are needed. The advent of dark-field microscopy (DFM) has enabled us to study the optical properties of single nanoparticles[9] and to analyse the effects of particle size, particle shape, the refractive index of the surrounding medium as well as the role of the substrate[9–12].

Figure 1a shows the DFM images of individual gold decahedra (orange) and triangular prisms (red) on a glass substrate, and Fig. 1b shows the gold rods and spheres. The spheres (~50 nm in diameter) scatter green light, whereas the rods, with a mean aspect ratio of 2.8, scatter red light. Particle agglomerates appear as white or yellow scattered light.

So far, most DFM investigations have focused on understanding the size- and shape-dependent optical properties of small metal particles. The goal is to extend these investigations to include the study of chemical reactions by combining DFM and surface plasmon spectroscopy (SPS). One such class of reaction includes nanoparticle-catalysed oxidative processes. For these reactions, it is necessary to be able to monitor the changes in electron densities of the individual particles throughout the catalytic cycle. It is a well-known fact that the SP resonances of metal nanocrystals are sensitive to perturbations such as electron charging[13]. According to the microelectrode model of redox catalysis[11,12], a small metal particle in a solution couples two redox reactions by acting as a reservoir for the electrons. In the first step, a donor molecule transfers the electrons to the nanocrystal (NC) through the following reaction:

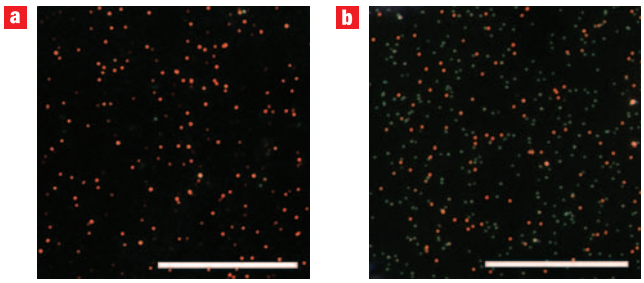

Figure 1 DFM images of gold nanocrystals of different shapes. **a**, Nanodecahedra and triangular prisms. **b**, Nanorods and 50-nm spheres. Scale bars, 50 μm.

$$D^- \rightarrow D + e^-_{NC} \quad (1)$$

These electrons are then transferred to the acceptor couple as given in the following reaction:

$$A + e^-_{NC} \rightarrow A^- \quad (2)$$

The particle catalyses the reaction if the rates of the above reactions are faster than the direct electron transfer from the donor, D^-, to the acceptor, A, in a bulk solution. The microelectrode model has been used successfully to explain many different types of catalytic reaction including enzyme catalysis[14], open circuit reactions on electrodes[15,16] and colloid catalysed hydrogen formation from water[4,17–19].

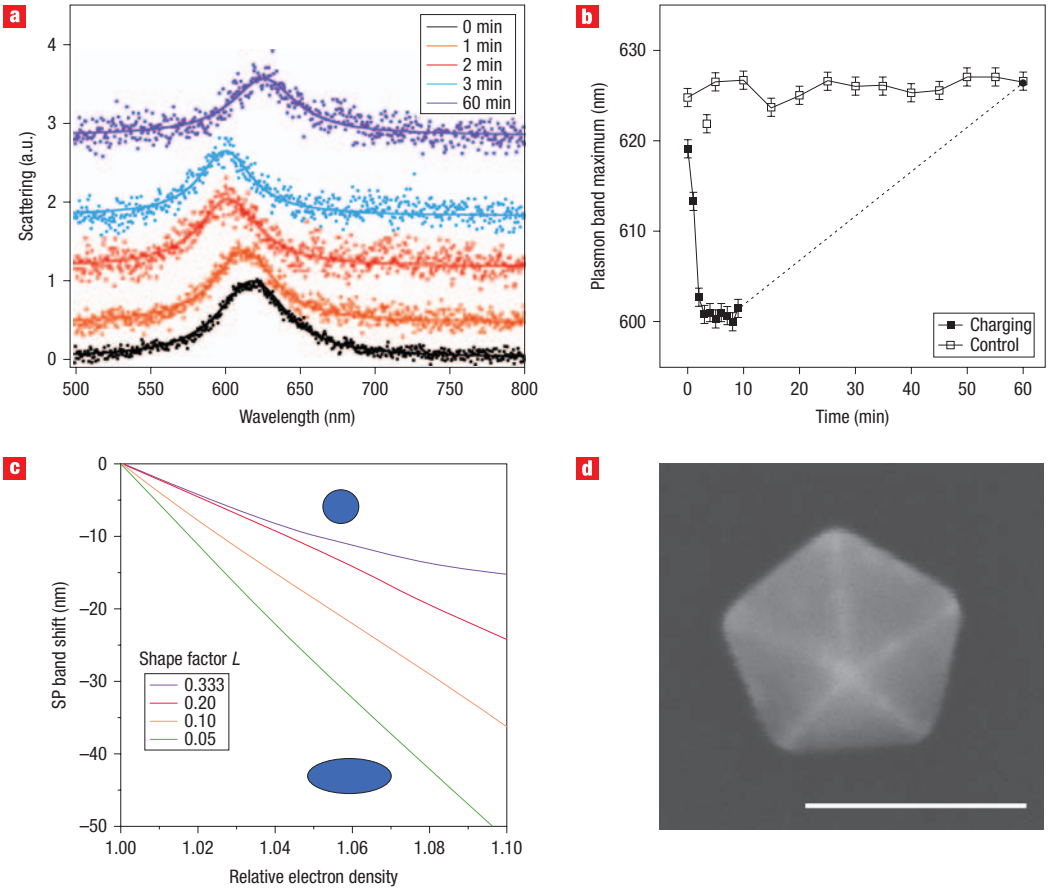

Figure 2 Gold-catalysed oxidation of ascorbic acid. a, Scattering spectra of the decahedron shown in Fig. 2d before and at 1, 2, 3 and 60 min after electron injection by ascorbate ions. **b**, Spectral shift as a function of time for the catalysis reaction and for the control experiment. The error bars represent the error in determining the peak position from the Lorentzian fitting procedure. **c**, Plot of the sensitivity of the SP resonance to changes in electron density for different shaped gold nanocrystals. The medium relative permittivity is $\varepsilon_m = 2.025$, and L is the depolarization factor, which describes the nanocrystal morphology. **d**, SEM image of the gold decahedron used in the catalysis experiments of Fig. 2a–c. Scale bar, 100 nm.

SPS enables us to detect the transferred electrons stored in a single catalyst particle and to quantify their concentration in real time. The stored electrons alter the plasma frequency of the metal, leading to a blueshift in both the extinction and scattered light spectra of the particle[13]. This enables us to monitor, for the first time, the steady-state charge on an individual particle. Within the dipole approximation, maximum light scattering from a small gold catalyst particle coincides with the peak wavelengths of the SP modes. The relationship between the observed shift in the SP peak wavelength, $\Delta\lambda$, and the change in the nanoparticle electron density, ΔN, has previously been derived from the Rayleigh equation and agrees well with the experimental data for the charging of bulk nanocrystal samples. This relationship is given by[20]

$$\Delta\lambda = \lambda - \lambda_0 = \lambda_p \sqrt{\frac{\varepsilon_\infty + ((1-L)/L)\varepsilon_m}{1 + \Delta N/N}} \qquad (3)$$

Here N is the electron density of the metal, ε_∞ the high-frequency dielectric constant of the metal (12.2 for gold), L the shape factor of the nanocrystal, λ_p the bulk plasma wavelength (131 nm for gold), λ_0 the position of the SP peak for the uncharged nanocrystal and ε_m the dielectric permittivity. Spectral shifts can be monitored with a time resolution of just a few seconds, allowing us to monitor the kinetics of electron injection into single nanocrystals in real time.

It is important to note that Rayleigh scattering is proportional to d^6, where d is the diameter of the particle. This limits the DFM technique to particles with dimensions >50 nm. Therefore, the work described here has been performed with particles having sizes of the order of tens of nanometres to provide a first approach to understanding catalytic reaction mechanisms. The method allows one to study the effects of different crystal geometries and crystal facets on the rates of catalysis. Functional gold catalysts, on the other hand, are of the order of 2–10 nm in size and do not scatter light efficiently enough to be detected using DFM with current CCD detectors. However, incremental improvements in the design of the detectors should enable us to eventually study the particles in this size regime.

We consider, for example, the gold-catalysed oxidation of ascorbic acid by dissolved oxygen. The direct electron transfer reaction is very slow in an aqueous solution. In the presence of a gold catalyst, electrons are injected into the nanoparticle by the ascorbic acid[21]. A colloid containing predominantly gold decahedra was used for this experiment. For this reason, we assume that the particle analysed was a decahedra, but the same method would apply for other shapes. Figure 2a shows the Rayleigh spectra for the single gold nanocrystal as a function of

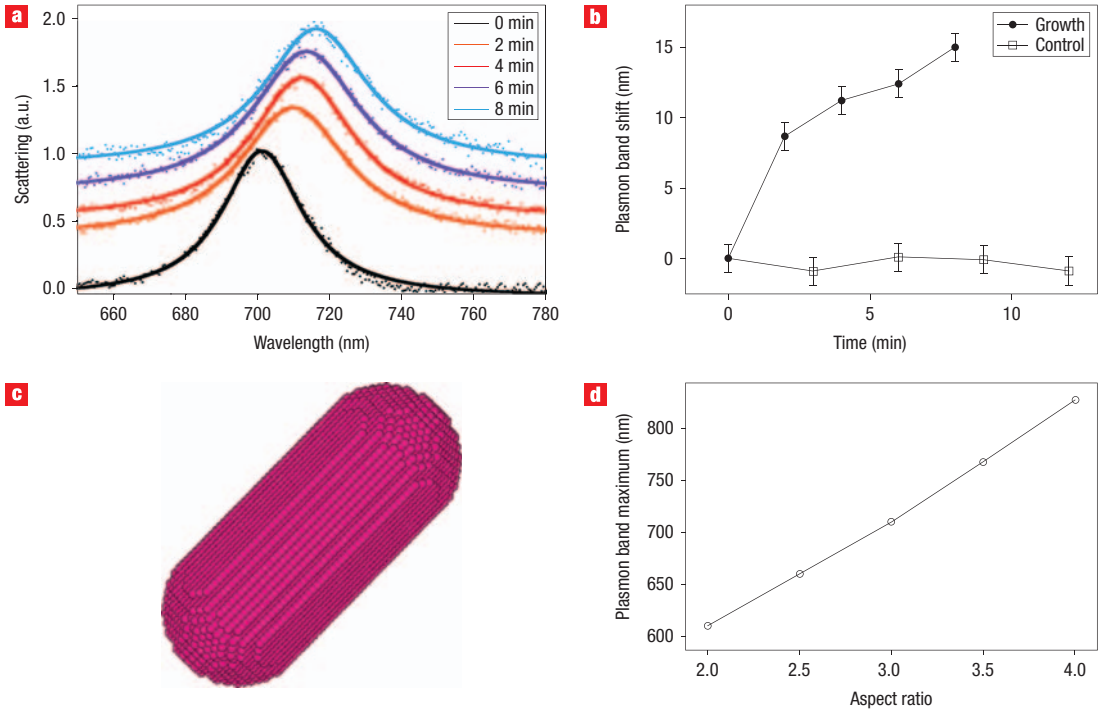

Figure 3 Growth of a single gold nanorod. a, Evolution of the scattering spectrum of a gold nanorod (aspect ratio 2.87) after a growth solution containing CTAB, $HAuCl_4$ and ascorbic acid (reducing agent) is added. Spectra are normalized and the full lines are the Lorentzian fits to the experimental data. **b**, SP band position as a function of time for the growth experiment and for a control experiment. The error bars represent the error in determining the peak position from the Lorentzian fitting procedure. **c**, Typical DDA target constructed to simulate hemispherically capped gold nanorods containing 52,000 dipoles and aspect ratio of 2.87. **d**, Predicted SP position versus aspect ratio for hemispherically capped rods in a medium with relative permittivity $\varepsilon_m = 2.025$ based on DDA results.

the reaction time. The SP band cyclically shifts ~ 20 nm during catalysis. A blueshift of the SP band is observed for more than 3 min as the electrons are injected[13,21,22], following which a plateau is reached where the gold particles have the highest electron density built up during the cycle. Following the plateau, the spectra then redshift back to the initial position of the SP band, as shown in the final 60-min spectrum. It is reasonable to consider that this shift reflects the electron density of the particle returning to its initial state and is due therefore to the discharge of the excess electrons from the particle through the reduction of oxygen to water. Following this reasoning then, the redshift occurs once the ascorbic acid has been oxidized:

$$Au_n + ze^- \rightarrow Au_n^{z-} \quad (4)$$

$$Au_n^{z-} + \frac{z}{4}O_2 + zH^+ \rightarrow Au_n + \frac{z}{2}H_2O \quad (5)$$

Oxygen discharge is quite slow because ascorbic acid initially reduces any oxygen present in the solution, and the oxygen must diffuse back into the solution to pick up the stored electrons. This facilitates the build up of a large negative charge on the decahedron before oxygen reduction can compete and, consequently, the gold catalyst accumulates an enormous steady-state electron density. A small decrease in the scattering intensity is also observed as the reaction proceeds and the spectra were therefore normalized for better visualization.

It is well known that changes in the refractive index of the surrounding medium, the temperature and the presence of dissolved gases can influence the scattering spectra of gold nanoparticles[10–12]. Control experiments were conducted under the same experimental conditions as the catalytic reaction but in the absence of ascorbic acid. The results are shown in Fig. 2b. In the absence of ascorbate ions, the spectra of individual nanoparticles on glass in water were observed to be very stable over time, indicating that the blueshift observed was caused exclusively by the electron injection.

Figure 2c shows the calculated spectral shifts for a gold particle as a function of the relative electron density, for a range of shape factors, using equation (3). The blueshift is almost linear but the slope is very sensitive to the shape of the particle. Spherical surfaces ($L = 0.33$) exhibit the weakest sensitivity, whereas elongated rods or other needle-like shapes with smaller depolarization factors exhibit the highest spectral shift per stored electron. For a small decahedron, L is ~ 0.17. To explain the observed blueshift from 620 to 600 nm, a 7% increase in electron density is required. An increase in the electron density of this size will result in a large negative potential on the gold cluster, bringing into question the possibility of other effects such as a shape change to the particle. The reversibility of the SP shift following the charge buildup, however, argues against this.

On the basis of high-resolution transmission electron microscopic images, it is found that a single decahedron in this sample contains $\sim 1 \times 10^7$ gold atoms (Fig. 2d). This means that $\sim$830,000 electrons would have to be added in 3 min, that is, 4,600 electrons per second, to cause such a blueshift. As the gold decahedron becomes negatively charged, the injection rate would be expected to decelerate as observed in Fig. 2a, whereas the rate of electron transfer from the cathodically charged catalyst particle to oxygen will gradually increase. The redshift because of oxygen reduction corresponds to a consumption of 65 O_2 molecules per second. These spectra constitute the first direct measurements of the rates of both steps of a redox reaction on a single nanocrystal.

The growth of gold nanoparticles with different morphologies from spherical gold seed particles is well known[23]. The gold atoms, produced by reduction of $AuCl_4^-$, deposit onto the facets with the lowest surface free energy. The stored electrons resulting from injection by ascorbic acid in the presence of cetyltrimethylammonium bromide (CTAB)[24–26] can also be used to reduce $AuCl_4^-$ to gold metal, which will deposit on the crystal faces of the single nanoparticles [equation (6)]. Gold rods provide an excellent test of this system, as deposition of even a small amount of gold metal on the rod tips, the lowest energy surface, will result in a relatively large redshift in the nanocrystal spectrum because of the change in the aspect ratio. Growth of particles of other shapes requires many more gold atoms to be deposited to produce similar redshifts in the spectrum:

$$Au_n^{z-} + \frac{z}{3}AuCl_4^- \rightarrow Au_{n+z/3} + \frac{4z}{3}Cl^- \qquad (6)$$

The above reaction has a much lower overpotential than reaction (5), so the steady-state charge on the gold catalyst is very small. However, an increase in the rod length causes the SP band to redshift because the shape factor L decreases as the rod grows[24,25]. Figure 3 shows the evolution of the spectrum of a single gold nanorod (of width 20 nm) upon reaction with $AuCl_4^-$ in the presence of ascorbic acid. Using the known shape factors for gold rods, determined by discrete dipole approximation (DDA) simulation[27], the peak position, shown in Fig. 3b, can be converted into a changing nanocrystal size, and the rod aspect ratio is found to be increased from 2.87 to 3.01. The increase in aspect ratio corresponds to the deposition of ~50,000 atoms for an 8-min reaction time or just ~100 atoms of gold every second.

In conclusion, we report the direct observation of redox reactions on single nanocrystals for the first time using DFM. Electron transfer rates of ~4,600 electrons per second can be directly measured and, in favourable cases, we have monitored chemical reaction rates of just 65 molecules of O_2 per second. The sensitivity is limited by the intrinsic SP band shift per electron added and by the current signal-to-noise collection efficiency of the CCD spectrometer. Improved signal-to-noise ratios open up the intriguing possibility of detecting the reactions of single molecules on nanocrystal surfaces and studying the quantum reaction regime, where the catalyst functions by accepting and transferring only one electron at a time.

METHODS

NANOCRYSTAL SYNTHESIS

Gold nanorods were synthesized following the seed-mediated growth method developed by Nikoobakht and El-Sayed[24]. Briefly, gold seeds were prepared by adding 5.0 ml of 0.00050 M $HAuCl_4$ to 5 ml of a 0.2 M CTAB solution. To this solution was added 0.6 ml of ice-cold $NaBH_4$ while stirring. A gold nanorod growth solution was prepared by adding 5 ml of 0.001 M $HAuCl_4$ to 5 ml of 0.2 M CTAB. To this mixture, 0.15 ml of 0.004 M $AgNO_3$ solution was added followed by the addition of 0.07 ml of 0.0788 M ascorbic acid. Finally, 0.012 ml of seed solution was added. The reaction takes ~1 h. The solution was centrifuged at 10,000 r.p.m. for 15 min to remove the excess CTAB and smaller spherical particles. The resulting solution was used as a stock solution in sample preparation. The colloid containing gold decahedra (70%) and trigonal prisms (30%) was synthesized using the seed-mediated growth method developed by Sánchez-Iglesias *et al.*[28].

SAMPLE PREPARATION

Glass slides were cleaned by sonication in dichloromethane, then acetone, then 10% NaOH and finally twice with Milli-Q water[29]. The stock gold nanoparticle solutions were diluted to half their original concentration using a 1% PVA in water solution. The mixture was spin cast onto clean, dry glass slides (30 μl, 3,000 r.p.m. for 5 s). The samples were allowed to dry for at least 5 min before being used. For the catalysed oxidation of ascorbic acid, a 0.558 M ascorbic acid solution was added dropwise onto the glass slide containing gold nanoparticles, and the spectrum of an individual nanoparticle was collected before and after the addition (every minute for 10 min, then after 60 min). As a control experiment, distilled water was added dropwise onto the glass slide containing gold nanoparticles, and the spectrum of an individual nanoparticle was collected every 5 min for 60 min. For the rod growth reaction, a growth solution containing 0.1 M CTAB, 8×10^{-5} M $AgNO_3$, 5×10^{-4} M $HAuCl_4$ and 5.52×10^{-5} M ascorbic acid was added dropwise onto the glass slide containing nanorods. The spectrum of an individual nanorod was collected every 2 min for 10 min. Spectra could not be collected further due to the crystallization of CTAB on the slide. The crystals, deposited on top of and among nanorods, scattered light very intensely, creating a too bright background. As a control experiment, distilled water was added dropwise onto a glass slide containing nanorods, and the spectrum of an individual rod was collected every 5 min for 60 min.

SINGLE-PARTICLE SPECTROSCOPY

Spectra of individual gold nanoparticles were recorded by collecting their scattered light with a Nikon Eclipse TE-2000 microscope coupled to a Nikon Dark-field Condenser, as described elsewhere[9]. The scattered light was collected by a Nikon Plan Fluor ELWD ×40/0.60 NA objective and focused onto the entrance port of a MicroSpec 2150i imaging spectrometer coupled with a TE-cooled CCD camera (PIXIS 1024B ACTON Princeton Instruments). The spectra were integrated for 60 s. The raw spectra were normalized for background light.

Received 13 May 2008; accepted 30 July 2008; published 14 September 2008.

References

1. Li, Y. & El-Sayed, M. A. The effect of stabilizers on the catalytic activity and stability of Pd colloidal nanoparticles in the Suzuki reactions in aqueous solution. *J. Phys. Chem. B* **105,** 8938–8943 (2001).
2. Meisel, D., Mulac, W. & Matheson, M. Catalysis of methyl viologen radical reactions by polymer-stabilized gold sols. *J. Phys. Chem.* **85,** 179–187 (1981).
3. Narayanan, R. & El-Sayed, M. A. Shape-dependent catalytic activity of platinum nanoparticles in colloidal solution. *Nano Lett.* **4,** 1343–1348 (2004).
4. Rupprechter, G. & Weilach, C. Mind the gap! Spectroscopy of catalytically active phases. *Nano Today* **2,** 20–29 (2007).
5. Park, I., Lee, K., Choi, J., Park, H. & Sung, Y. Surface structure of Pt-modified Au nanoparticles and electrocatalytic activity in formic acid electro-oxidation. *J. Phys. Chem. C* **111,** 19126–19133 (2007).
6. Chen, X. & Moskovits, M. Observing catalysis through the agency of the participating electrons: surface-chemistry-induced current changes in a tin oxide nanowire decorated with silver. *Nano Lett.* **7,** 807–812 (2007).
7. Fierro-Gonzalez, J. & Gates, B. Evidence of active species in CO oxidation catalyzed by highly dispersed supported gold. *Catal. Today* **122,** 201–210 (2007).
8. Somorjai, G., York, R., Butcher, D. & Park, J. The evolution of model catalytic systems: studies of structure, bonding and dynamics from single-crystal metal surfaces to nanoparticles, and from low pressure ($<10^{-3}$ Torr) to high pressure ($>10^{-3}$ Torr) to liquid interfaces. *Phys. Chem. Chem. Phys.* **9,** 3500–3513 (2007).
9. Novo, C. *et al.* Contributions from radiation damping and surface scattering to the linewidth of the longitudinal plasmon band of gold nanorods: a single particle study. *Phys. Chem. Chem. Phys.* **8,** 3540–3546 (2006).
10. Novo, C., Funston, A. M., Pastoriza-Santos, I., Liz-Marzán, L. & Mulvaney, P. Spectroscopy and high-resolution microscopy of single nanocrystals by a focused ion beam registration method. *Angew. Chem. Int. Ed.* **46,** 3517–3520 (2007).
11. Henglein, A. Physicochemical properties of small metal particles in solution—microelectrode reactions, chemisorption, composite metal particles, and the atom-to-metal transition. *J. Phys. Chem.* **97,** 5457–5471 (1993).
12. Bard, A., Crayston, J., Kittlesen, G., Shea, T. & Wrighton, M. Digital simulation of the measured electrochemical response of reversible redox couples at microelectrode arrays—consequences arising from closely spaced ultramicroelectrodes. *Anal. Chem.* **58,** 2321–2331 (1986).
13. Mulvaney, P. Surface plasmon spectroscopy of nanosized metal particles. *Langmuir* **12,** 788–800 (1996).
14. Bockris, J., Damjanov, A. & Mannan, R. Catalysis of electrodic hydrogen evolution and dissolution reactions on rationally chosen substrates. *J. Electroanal. Chem.* **18,** 349–361 (1968).
15. Spiro, M. & Freund, P. Colloidal catalysis—transport versus surface control. *J. Chem. Soc., Faraday Trans. I* **79,** 1649–1658 (1983).

16. Spiro, M. Heterogeneous catalysis in solution. 17. Kinetics of oxidation–reduction reactions catalyzed by electron-transfer through the solid—an electrochemical treatment. *J. Chem. Soc., Faraday Trans. I* **75,** 1507–1512 (1979).
17. Henglein, A. & Lilie, J. Storage of electrons in aqueous solution—the rates of chemical charging and discharging the colloidal silver microelectrode. *J. Am. Chem. Soc.* **103,** 1059–1066 (1981).
18. Miller, D., Bard, A., McLendon, G. & Ferguson, J. Catalytic water reduction at colloidal metal microelectrodes. 2. Theory and experiment. *J. Am. Chem. Soc.* **103,** 5336–5341 (1981).
19. Kiwi, J. & Gratzel, M. Hydrogen evolution from water induced by visible light mediated by redox catalysis. *Nature* **281,** 657–658 (1979).
20. Mulvaney, P., Perez-Juste, J., Giersig, M., Liz-Marzán, L. & Pecharroman, C. Drastic surface plasmon mode shifts in gold nanorods due to electron charging. *Plasmonics* **1,** 61–66 (2006).
21. Novo, C. & Mulvaney, P. Charge-induced Rayleigh instabilities in small gold rods. *Nano Lett.* **7,** 520–524 (2007).
22. Mulvaney, P., Linnert, T. & Henglein, A. Surface chemistry of colloidal silver in aqueous solution—observations on chemisorption and reactivity. *J. Phys. Chem.* **95,** 7843–7846 (1991).
23. Liz-Marzán, L. Tailoring surface plasmons through the morphology and assembly of metal nanoparticles. *Langmuir* **22,** 32–41 (2006).
24. Nikoobakht, B. & El-Sayed, M. A. Preparation and growth mechanism of gold nanorods (NRs) using seed-mediated growth method. *Chem. Mater.* **15,** 1957–1962 (2003).
25. Perez-Juste, J., Liz-Marzán, L., Carnie, S., Chan, D. & Mulvaney, P. Electric-field-directed growth of gold nanorods in aqueous surfactant solutions. *Adv. Funct. Mater.* **14,** 571–579 (2004).
26. Jana, N., Gearheart, L. & Murphy, C. Wet chemical synthesis of silver nanorods and nanowires of controllable aspect ratio. *Chem. Commun.* 617–618 (2001).
27. Prescott, S. & Mulvaney, P. Gold nanorod extinction spectra. *J. Appl. Phys.* **99,** 123504-1 (2006).
28. Sánchez-Iglesias, A. *et al.* Synthesis and optical properties of gold nanodecahedra with size control. *Adv. Mater.* **18,** 2529–2534 (2006).
29. Gesquiere, A., Park, S. & Barbara, P. F-V/SMS: a new technique for studying the structure and dynamics of single molecules and nanoparticles. *J. Phys. Chem. B* **108,** 10301–10308 (2004).

Acknowledgements

C.N. thanks the University of Melbourne for MIRS and MIFRS postgraduate scholarships and P.M. thanks the ARC for support through FF 0561456. We acknowledge I. Pastoriza-Santos for the gold pentagon samples.

Author contributions

C.N. performed the experiments and analysed the data together with P.M. and A.M.F. A.M.F. provided help with the optics. All authors discussed the results and co-wrote the manuscript.

Author information

Reprints and permission information is available online at http://npg.nature.com/reprintsandpermissions/. Correspondence and requests for materials should be addressed to P.M.